Journal of Alloys and Compounds 509 (2011) L63–L68

Contents lists available at ScienceDirect

Journal of Alloys and Compounds

journal homepage: www.elsevier.com/locate/jallcom

Letter

Novel fabrication of forsterite scaffold with improved mechanical properties

H. Ghomi*, M. Jaberzadeh, M.H. Fathi

Biomaterials Group, Department of Materials Engineering, Isfahan University of Technology, Isfahan 8415683111, Iran

ARTICLE INFO

Article history:
Received 31 July 2010
Received in revised form 10 October 2010
Accepted 24 October 2010
Available online 3 November 2010

Keywords:
Ceramics
Nanostructured materials
Mechanical alloying
Mechanical properties
Scanning electron microscopy
X-ray diffraction

ABSTRACT

In this study, the macroporous forsterite scaffolds with highly interconnected spherical pores, with sizes ranged from 50 to 200 μm have been successfully fabricated via gelcasting method. The crystallite size of the forsterite scaffolds was measured in the range 26–35 nm. Total porosity of different bodies sintered at different sintering temperatures was calculated in the range 81–86%, while open porosity ranges from 69 to 78%. The maximum values of compressive strength and elastic modulus of the prepared scaffolds were found to be about 2.43 MPa and 182 MPa, respectively, which are close to the lower limit of the compressive strength and elastic modulus of cancellous bone and the compressive strength is equal to the standard for a porous bioceramic bone implant (2.4 MPa). Transmission electron microscopy analyses showed that the particle sizes are smaller than 100 nm. In vitro test in the simulated body fluid proved the good bioactivity of the prepared scaffold. It seems that, the mentioned properties could make the forsterite scaffold appropriate for tissue engineering applications, but cell culture and in vivo tests are needed for more confidence.

1. Introduction

Bioceramics as a class of biomaterials are very important for biomedical applications [1]. Porous bioceramic devices or implants have been paid much attention. In fact, porous bioceramics have been used for bone defect filling, implant fixation via bone ingrowth (i.e. biological fixation), bone regeneration via tissue engineering [2–4], drug delivery [5–8], cell loading [9,10], and ocular implant [11]. However, it is challenging to control and optimize the porous structures (e.g. porosity, pore size, and pore interconnectivity) and the mechanical properties of porous bioceramics.

In recent years, some Si and Mg containing ceramics have drawn interests in the development of bone implant materials [12–18]. Silicon was known as an essential element in skeletal development. It was uniquely localized in the active areas of young bone and was involved in the early stage of bone calcification [19,20]. Magnesium is also certainly one of the most important elements in human body, associated with mineralization of calcined tissues [21], and indirectly influences mineral metabolism [22]. Forsterite (Mg_2SiO_4) is an important material of olivine family of crystals in the magnesia–silica system. Recently researches have shown that it is a biocompatible material, possess excellent in vitro apatite-formation ability, in vivo bioactivity and degradability [23–29], improved mechanical properties compared to hydroxyapatite [28], and can be useful as a biomaterial for hard tissue repair. Forsterite ceramics have shown a significant improvement in the fracture toughness (K_{IC} = 2.4 MPa $m^{1/2}$) in comparison to hydroxyapatite ceramics (0.6–1.0 MPa $m^{1/2}$) [23,30,31]. Preparing the nanocrystalline forsterite dense ceramics via sintering the forsterite nanopowder suggests that these can be significantly improved concerning their fracture toughness (K_{IC} = 3.61 MPa $m^{1/2}$) and hardness (940 Hv) in comparison to the hydroxyapatite ceramics (K_{IC} = 0.75–1.2 MPa $m^{1/2}$ and hardness = 700 Hv) [32]. Despite the advantages of forsterite in comparison to other bioceramic, such as its good mechanical properties, there are not any published reports on fabrication of porous forsterite.

Nanoparticle ceramics in comparison to microparticle ceramics have a number of attractive properties which includes high mechanical properties, high diffusion rates, and reduced sintering times or temperatures [33–36]. Studies on nanostructure bioceramic such as alumina, titania, and hydroxyapatite have illustrated enhanced adhesion of osteoblast cells, and decreased adhesion of fibroblast and endothelial cells [37].

Present study was aimed to produce and characterize porous body of nanostructure forsterite for tissue engineering applications in order to impart of its high mechanical properties. For this purpose, forsterite nanopowder was synthesized using the mechanical activation method and porous body of forsterite was fabricated via the gelcasting method. Gelcasting method is a well-established method in which the foaming was conducted by addition of a foaming agent and vigorous agitation of aqueous ceramic suspension. Then in situ polymerization of an organic monomer [38] or gelation of a gelling agent [39,40] cause to form a sufficiently strong

* Corresponding author. Tel.: +98 311 3912750; fax: +98 311 3912752.
E-mail address: hamed1985.gh@gmail.com (H. Ghomi).

0925-8388/$ – see front matter © 2010 Elsevier B.V. All rights reserved.
doi:10.1016/j.jallcom.2010.10.106

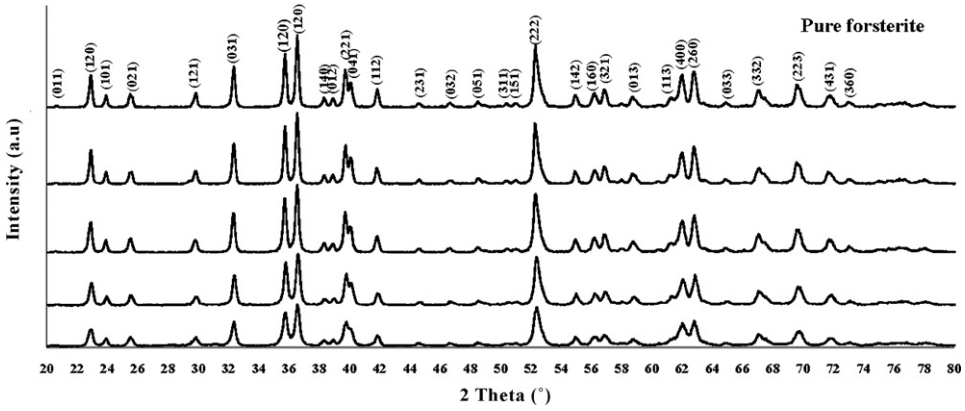

Fig. 1. XRD patterns of the prepared (a) forsterite nanopowder, and forsterite scaffolds sintered at (b) 900, (c) 1000, (d) 1100, and (d) 1200 °C for 4 h.

gel to withstand the body weight, even at the typically low solids loading used in these suspensions.

2. Experimental procedure

2.1. Starting materials

Magnesium carbonate ($MgCO_3$, Aldrich, 98% purity) and talc ($Mg_3Si_4O_{10}(OH)_2$, Merck, 98% purity) powders were used as raw materials to prepare forsterite powder. In order to fabricate the porous body of the forsterite, agarose powder (Merck) as a gelling agent, Tergitol Np-9 (Aldrich) as a foaming agent, and tripoly phosphate sodium (TPP) as a dispersant were used in gelcasting process.

2.2. Preparation of nanostructure forsterite

In order to produce a single phase forsterite, $MgCO_3$ and talc powders with molar ratio of 5:1 were mixed in a planetary ball mill under ambient conditions. The milling media consisted of a zirconia vial with zirconia balls. In milling process, the rotational speed of main disc was 350 rpm, the ball-to-powder weight ratio was 10:1 and the time of mechanical activation was 10 h. The prepared powder was then heated at 1000 °C for 1 h in air.

2.3. Fabrication of porous body of the forsterite

Forsterite powder was dispersed in deionized water by using of 1 wt% tripoly phosphate sodium as a dispersant and a slurry of 60 wt% solid loading was prepared. The amount of 7 wt% agarose powder as a gelling agent was dissolved in deionized water by heating the water up to 130 °C. The agarose solution by keeping the temperature of the initial slurry at 80 °C was added to the forsterite slurry. Then 1.5 vol.% Tergitol as a surfactant was added to prepared suspension, with 50 wt% forsterite and 1.2 wt% active gelling agent. The suspension was then foamed through vigorous agitation by a triple-blade mixer. The foamed slurry was poured into the polyethylene mold and was cooled to 0 °C to gel the suspension. The samples were then de-molded, dried at room temperature, and sintered at different temperatures.

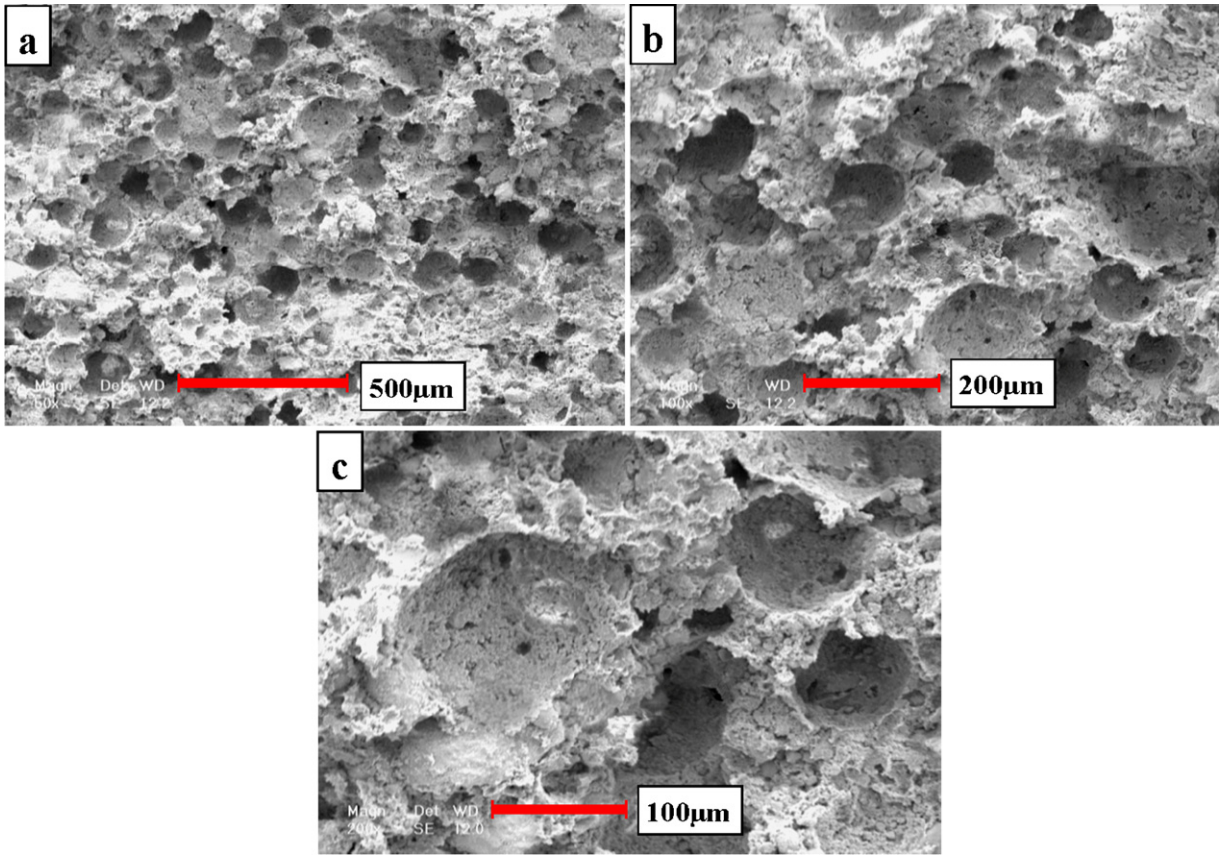

Fig. 2. SEM micrographs of the prepared forsterite scaffold sintered at 1200 °C for 4 h at different magnifications.

2.4. Materials characterization

The phase structure of the prepared forsterite powder and porous body of the forsterite were investigated by X-ray diffractometer (XRD, Philips Xpert) with Cu Kα radiation (λ = 0.154056 nm). The XRD patterns were recorded in the 2θ range of 20–80° (step size: 0.05° and time per step: 1 s).

The Scherrer's method was used to estimate the crystallite size of the forsterite powder and the prepared scaffolds [41].

$$d = \frac{(0.89\lambda)}{(B\cos\theta)} \quad (1)$$

where d is the crystallite size (nm), λ is the wavelength of the radiation used (nm), B is the diffraction peak width at half maximum intensity (rad), and θ is the Bragg diffraction angle (°).

The morphology and size of the pores in the prepared scaffolds were studied by scanning electron microscopy (SEM) in a Philips XL30.

Transmission electron microscopy (TEM, Philips CM-200) technique was utilized to characterize the morphology and particle sizes of the synthesized forsterite scaffolds.

The porosity and density of the samples were determined using the Archimedes method with distilled water as an immersion medium and using the theoretical density of 3.221 g cm^{-3} for forsterite [42]. The results are the average of three measurements for each sintering temperatures.

The mechanical behavior of the prepared scaffolds was investigated by compressive tests performed on cylindrical bars (10 mm in diameter and 20 mm in length) using a universal testing machine (zwick, material prufung, 1446-60). A crosshead speed of 0.5 mm/min was used for this purpose and the maximum force registered during the test was used for measuring the compressive strength of the scaffolds. The results are the average of five measurements for each sintering temperatures.

In vitro bioactivity of the prepared forsterite scaffolds was investigated by soaking them in the simulated body fluid (SBF) at a solid/liquid ratio of 10 mg/ml without refreshing the soaking medium. The SBF solution was prepared with the composition described by Kokubo and Takadama [43]. The samples were immersed in appropriate amount of SBF in plastic bottles and hold in a water bath at 36.5 ± 0.5 °C for 28 days. The samples were then filtered, rinsed with distilled water and dried in air. The formation of the apatite layer on the samples was confirmed using SEM micrographs. The changes in pH value of soaking solutions were also measured using an electrolyte-type pH meter every day.

3. Results and discussion

The XRD patterns of the starting powder and porous forsterite pieces sintered at different temperatures are shown in Fig. 1. Good agreement was found between the XRD pattern obtained from forsterite powder (Fig. 1a) and the standards for forsterite, compiled by the Joint Committee on Powder Diffraction and Standards (JCPDS). Porous pieces after sintering were ground into powder. Compared with the card 34-0189, there were no phase transformations detected when the sintering temperature was increased to 1200 °C. The broad peak width of the diffraction patterns could be attributed to the small crystal size. The crystallite size of the prepared forsterite powder was measured about 23 nm by broadening of XRD peaks using Scherrer's formula. However, when the sintering temperature was increased to 1200 °C, the crystallite size was increased to 35 nm.

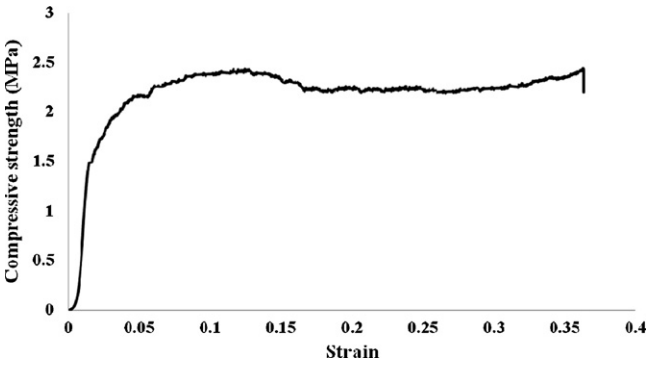

Fig. 3. Compressive stress–strain curve of the forsterite scaffold sintered at 1200 °C for 4 h.

Scanning electron micrographs of the sintered porous bodies of forsterite are shown in Fig. 2. Fig. 2 is related to the scaffold sintered at 1200 °C for 4 h at different magnifications. These Figures show that the scaffolds have an open, interconnected, and uniform porous microstructure with pore sizes ranged from 50 to 200 μm. Observations by SEM showed a decrease in pore size with an increase in the sintering temperature.

Total porosity of different bodies sintered at different sintering temperatures ranges from 81 to 86%, while open porosity ranges from 69 to 78%. When sintering temperature is raised from 900 to 1200 °C, total porosity of the samples decreases by 5% and open porosity by as much as 9%.

Table 1 show the crystallite size, total porosity, apparent density, elastic modulus, and compressive strength of the scaffolds sintered at different temperatures. The compression tests showed that all the samples failed in a manner similar to that for brittle ceramic foams, exhibiting linear elastic region followed by a collapse plateau presumably dominated by brittle fracture of the

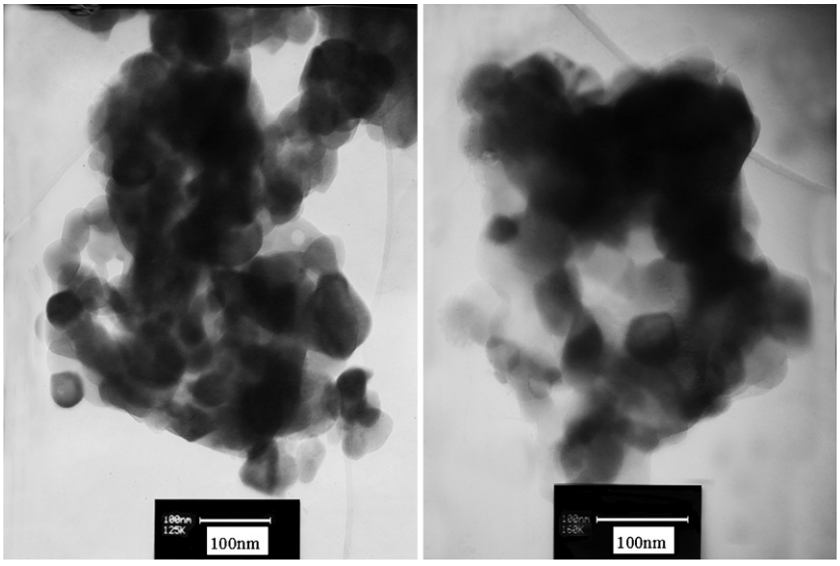

Fig. 4. TEM micrographs of the forsterite scaffold sintered at 1200 °C for 4 h at different magnifications.

Table 1
The crystallite size, total porosity, apparent density, elastic modulus, and compressive strength of the forsterite scaffolds at different sintering temperatures.

Temperature	Crystallite size (nm) (S.D.[a])	Apparent density)gr cm^{-3}) (S.D.)	Total porosity (%) (S.D.)	Compressive strength (MPa) (S.D.)	Elastic modulus (MPa) (S.D.)
Forsterite powder	23 (±1)	3.14 (±0.1)	–	–	–
900 °C	26 (±2)	0.45 (±0.04)	86 (±1)	2.06 (±0.09)	145 (±9)
1000 °C	28 (±1)	0.48 (±0.08)	85 (±1)	2.19 (±0.06)	165 (±12)
1100 °C	31 (±1)	0.55 (±0.05)	83 (±2)	2.31 (±0.07)	171 (±21)
1200 °C	35 (±2)	0.61 (±0.06)	81 (±1)	2.43 (±0.11)	182 (±19)

[a] Standard deviation.

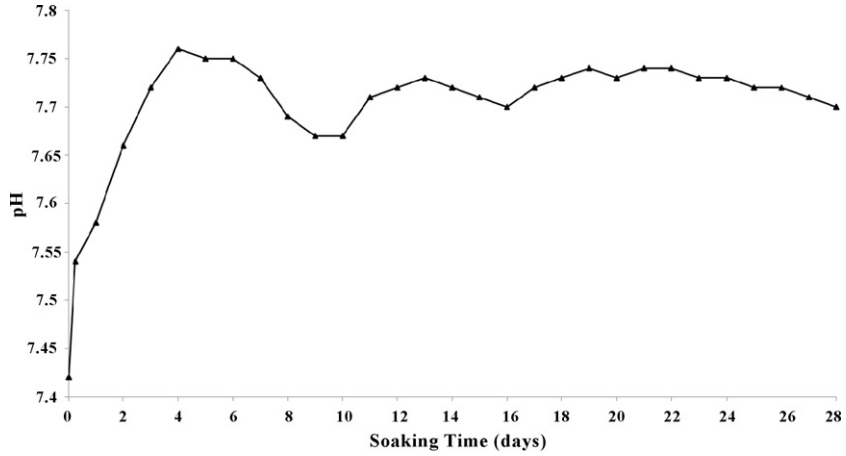

Fig. 5. Changes of pH of the SBF solution after soaking the forsterite scaffold for various periods.

struts. Fig. 3 is a typical example of compressive stress–strain curve for the forsterite scaffolds with porosity level of 81%. Both the compressive strength and elastic modulus of the scaffolds increased with increasing sintering temperature, due to a decrease in pore size and increases the density of the scaffolds. The elastic modulus ranged from 145 to 182 MPa, which is roughly equal to the low range of the values for spongy bone (~0.05–0.5 GPa) [44,45]. The compressive strength of the forsterite scaffolds was found in the

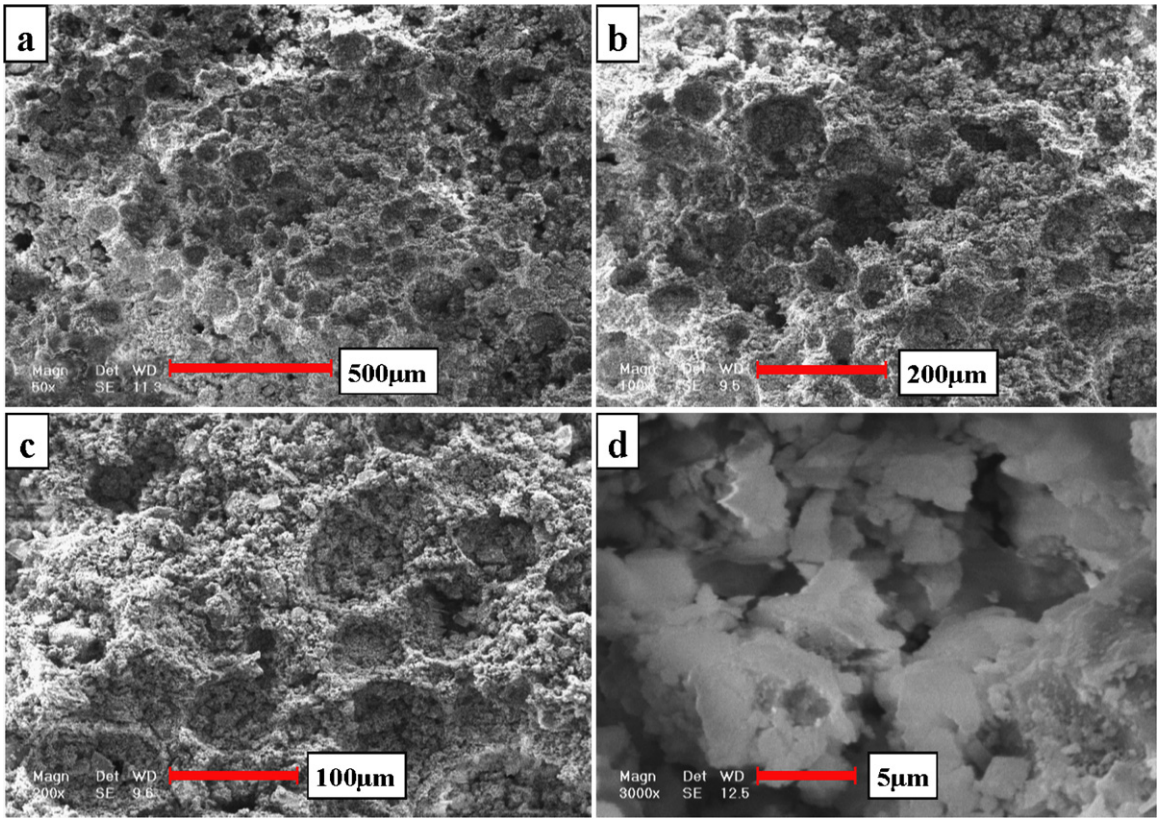

Fig. 6. SEM micrographs of the forsterite scaffold sintered at 1200 °C for 4 h after 28 days of immersion in the SBF at different magnifications.

range 2.06–2.43 MPa, which is close to the lower limit of the compressive strength of cancellous bone (2–12 MPa) [46] and is equal to the standard for a porous bioceramic bone implant (2.4 MPa) [47]. In comparison to the result of other researcher for prepared scaffolds of different bioceramics such as HA, TCP, and BG [39,40,48–50], the scaffolds compressive strength have increased by using the nano forsterite as a bioceramic.

Observation under TEM (Fig. 4, for the sample sintered at 1200 °C for 4 h) illustrated the apparent agglomerates of about 100 nm in size, upon close inspection reveal sub-structure of nano crystals of about 23–35 nm in size.

In vitro bioresorbability behavior of the prepared forsterite scaffold was quantitatively evaluated in the SBF medium under physiological condition of pH 7.4 at 36.5 ± 0.5 °C at pre-determined time intervals up to 28 days. Fig. 5 shows a graph of the changes of pH versus time, which illustrates the dissolution or resorbability behavior of synthesized samples. The pH value is dependent on the solubility or resorbability of the bioceramic. When the porous body of forsterite is immersed in the SBF, magnesium ions first exchange with H^+ in the solution lead to the formation of silanol ($Si–OH^-$) in the surface layer, a pH increase, and eventually the production of a negatively charged surface with the functional group ($Si–OH^-$). The calcium ions in the SBF solution are firstly attracted to the interface between the scaffold and solution. Calcium accumulating on the silica-rich layer lead to decreasing of phosphorus concentration in the SBF and presence of enough calcium and phosphorus on the forsterite scaffold cause formation of apatite layer on the surface [50].

The bone-like apatite formation on the surface of the prepared scaffold due to the dissolution and precipitation process of calcium phosphate after 28 days of immersion in the SBF are shown in Fig. 6. These SEM photomicrographs illustrated the formation of bone-like apatite (shiny regions) on the surface of the scaffold and pores filling by formation of apatite [24].

In recent years, particular attention has been paid to the preparation of bioceramics with porous morphology [2]. Since, the porous bioceramic have poor mechanical properties that limit their application in tissue engineering, it is very important to increase the mechanical properties of porous bioceramics. In this study, the using of forsterite as a bioceramic in addition to its nanostructure, increased the compressive strength of prepared scaffold in comparison to other porous bioceramic, and could make the prepared scaffold some applicable for load-bearing tissue engineering. In addition, bone tissue grows well into the pores, could increase strength of the prepared scaffold.

The manufactured forsterite scaffold, because of its sufficient compressive strength, pore size, and interconnectivity between pores, might be suitable for tissue engineering applications.

Further studies will be focused on cell culture and in vivo tests on the prepared scaffolds.

4. Conclusions

In this study, the macroporous forsterite scaffolds with highly interconnected spherical pores, with sizes ranged from 50 to 200 μm have been successfully fabricated via gelcasting method. The crystallite size of the forsterite scaffolds was measured in the range 26–35 nm. Total porosity of different bodies sintered at different sintering temperatures was calculated in the range 81–86%, while open porosity ranges from 69 to 78%. The maximum values of compressive strength and elastic modulus of the prepared scaffolds were found to be about 2.43 MPa and 182 MPa, respectively, which are close to the lower limit of the compressive strength and elastic modulus of cancellous bone and the compressive strength is equal to the standard for a porous bioceramic bone implant (2.4 MPa). TEM analyses showed the particle sizes are smaller than 100 nm. In vitro test in the simulated body fluid proved the good bioactivity of the prepared scaffold. It seems that, the mentioned properties could make the forsterite scaffold appropriate for tissue engineering applications, but cell culture and in vivo tests are needed for more confidence. Furthermore, its sufficient compressive strength could make it a good candidate for load-bearing tissue engineering.

Acknowledgement

The authors are grateful to Isfahan University of Technology for supporting this research.

References

[1] S. Oh, N. Oh, M. Appleford, J.L. Ong, Bioceramics for tissue engineering applications, Am. J. Biochem. Biotechnol. 2 (2006) 49–56.
[2] I. Sopyan, M. Mel, S. Ramesh, K.A. Khalid, Sci. Technol. Adv. Mater. 8 (1–2) (2007) 116–123.
[3] Z.C. Qizhi, D.T. Ian, R.B. Aldo, Biomaterials 27 (2006) 2414–2425.
[4] L.L. Hench, J. Am. Ceram. Soc. 81 (7) (1998) 1705–1728.
[5] A. Krajewski, A. Ravaglioli, E. Roncari, P. Pinasco, J. Mater. Sci.: Mater. Med. 12 (2000) 763–771.
[6] D.J.A. Netz, P. Sepulveda, V.C. Pandolfelli, A.C.C. Spadaro, J.B. Alencastre, M.V.L.B. Bentley, et al., Int. J. Pharm. 213 (1–2) (2001) 117–125.
[7] S. Hesaraki, F. Moztarzadeh, N. Nezafati, Med. Eng. Phys. 31 (10) (2009) 1205–1213.
[8] M. Itokazu, M. Esaki, K. Yamamoto, T. Tanemori, T. Kasai, J. Mater. Sci.: Mater. Med. 10 (1999) 249–252.
[9] H. Ohgushi, A.I. Caplan, J. Biomed. Mater. 48 (1999) 913–927.
[10] A. Banfi, A. Muraglia, B. Dozin, M. Mastrogiacomo, R. Cancedda, R. Quarto, Exp. Hematol. 28 (2000) 707–715.
[11] B. Kundu, M.K. Sinha, M.K. Mitra, D. Basu, Bull. Mater. Sci. 27 (2) (2004) 133–140.
[12] C.C. Mardare, A.I. Mardare, J.R.F. Fernandes, E. Joanni, S.C.A. Pina, M.H.V. Fernandes, et al., J. Eur. Ceram. Soc. 23 (2003) 1027–1030.
[13] C. Vitale-Brovarone, S. Dinunzio, O. Bretcanu, E. Verne, J. Mater. Sci. Mater. Med. 15 (2004) 209–217.
[14] T. Kobayashi, K. Okada, T. Kuroda, K. Sato, J. Biomed. Mater. Res. 37 (1997) 100–107.
[15] C.T. Wu, J. Chang, Mater. Lett. 58 (2004) 2415–2417.
[16] H.S. Ryu, K.S. Hong, J.K. Lee, D.J. Kim, J.H. Lee, Biomaterials 25 (2004) 393–401.
[17] S.R. Kim, J.H. Lee, Y.T. Kim, D.H. Riu, S.J. Jung, Y.J. Lee, et al., Biomaterials 24 (2003) 1389–1398.
[18] T.J. Webster, E.A. Massa-Schlueter, J.L. Smith, E.B. Slamovich, Biomaterials 25 (2004) 2111–2121.
[19] E.M. Carlisle, Science 167 (1970) 279–280.
[20] K. Schwarz, D.B. Milne, Nature 239 (1972) 333–334.
[21] R.Z. LeGeros, Calcium Phosphates in Oral Biology and Medicine, Basel, Switzerland, 1991.
[22] J. Althoff, P. Quint, E.R. Krefting, H.J. Hohling, Histochemistry 74 (1982) 541–552.
[23] M. Kharaziha, M.H. Fathi, J. Mech. Behav. Biomed. Mater. 7 (2010) 530–537.
[24] M. Kharaziha, M.H. Fathi, J. Alloys Compd. 472 (2008) 540–545.
[25] M. Kharaziha, M.H. Fathi, Ceram. Int. 35 (2009) 2449–2454.
[26] C. Wu, J. Chang, J. Biomed. Mater. Res. B: Appl. Biomater. 83 (1) (2007) 153–160.
[27] Y. Miake, T. Yanagisawa, Y. Yajima, H. Noma, N. Yasui, T. Nonami, J. Dent. Res. 74 (11) (1995) 1756–1763.
[28] T. Nonami, S. Tsutsumi, J. Mater. Sci. 10 (8) (1999) 475–479.
[29] T. Kobayashi, K. Okada, T. Kuroda, K. Sato, J. Biomed. Mater. Res. 37 (1) (1997) 100–107.
[30] S. Ni, L. Chou, J. Chang, Ceram. Int. 33 (2007) 83–88.
[31] F. Tavangarian, R. Emadi, J. Alloys Compd. 485 (2009) 648–652.
[32] M.H. Fathi, M. Kharaziha, Mater. Lett. 63 (2009) 1455–1458.
[33] M. Tavoosi, M.H. Enayati, F. Karimzadeh, J. Alloys Compd. 464 (2008) 107–110.
[34] L. Zhenglong, L. Zuyan, C. Yanbin, J. Alloys Compd. 470 (2009) 470–472.
[35] G.L. Tan, J.H. Du, Q.J. Zhang, J. Alloys Compd. 468 (2009) 421–431.
[36] K.P. Sanosh, A. Balakrishnana, L. Francis, T.N. Kim, J. Alloys Compd. 495 (2010) 113–115.
[37] T.J. Webster, R.W. Siegel, R. Bizios, Biomaterials 20 (1999) 1221–1227.
[38] P. Sepulveda, F.S. Ortega, M.D.M. Innocentini, V.C. Pandolfelli, J. Am. Ceram. Soc. 83 (12) (2000) 3021–3024.
[39] M. Potoczek, Mater. Lett. 62 (6–7) (2008) 1055–1057.
[40] M. Potoczek, A. Zima, Z. Paszkiewicz, A. Slosarczyk, Ceram. Int. 35 (2009) 2249–2254.
[41] B.D. Cullity, Elements of X-Ray Diffracton, 2nd ed, Addison-Wesley, 1978.
[42] Ji Sh, Z. Wang, Geodynamics 28 (1999) 147–174.

[43] T. Kokubo, H. Takadama, Biomaterials 27 (2006) 2907–2915.
[44] J.D. Currey, Clin. Orthop. Relat. Res. 73 (1970) 210–231.
[45] L.L. Hench, J. Wilson, An Introduction to Bioceramics, World Scientific, Singapore, 1993.
[46] D.R. Carter, W.C. Hayes, Science 194 (1976) 1174–1176.
[47] Implants for surgery-hydroxyapatite-Part1: ceramic hydroxyapatite, BS ISO 13779-1:2000.
[48] J.R. Jones, L.L. Hench, J. Mater. Sci. 38 (18) (2003) 3783–3790.
[49] H.R. Ramay, M. Zhang, Biomaterials 24 (2003) 3293–3302.
[50] C. Wu, J. Changa, J. Wang, S. Ni, W. Zhai, Biomaterials 26 (2005) 2925–2931.